Liquid immiscibility recorded in melt inclusions within corundum from alkaline basalt, Changle area, Shandong province, Eastern China

LIU JiQiang[1], NI Pei[1*], SHEN Kun[2] and DING JunYing[1]

1. *State Key Laboratory for Mineral Deposit Research, Institute of Geo-Fluids, Deportment of Earth Science , Nanjing University, Nanjing* 210093, *China*
2. *Shandong Institute and Laboratory of Geological Sciences, Jinan* 250013, *China*
Received: 2006-07-2 Accepted: 2006-11-10

Liu JQ, Ni P, Shen K and Ding JY. 2007. Liquid immiscibility recorded in melt inclusions within corundum from alkaline basalt, Changle area, Shandong province, Eastern China. *Acta Petrologica Sinica*, 23(1):125 – 130

Abstract Abundant melt- and fluid inclusions occur in corundum megacrysts of alkaline basalt from the Changle area, Shandong province, eastern China. One type of melt inclusions, i. e. multiphase melt inclusions (glass + bubbles + daughter minerals) were identified ,which occur along growth zones of host corundum megacrysts. Microthermometry and laser Raman microprobe analysis were performed on the melt inclusions. The bubbles within the melt inclusions are confirmed to be CO_2-rich phase and the daughter minerals are probably silicates, such as augite and okenite. The results of high temperature homogenization experiment strongly suggest that two immiscible melts, i. e. a H_2O- and CO_2-rich melt and an anhydrous and CO_2-poor melt were trapped by melt inclusions in corundum megacryst.

Key words Melt inclusion, Immiscibility, Corundum, Alkaline basalt, Changle area, Eastern China

Study of melt and fluid inclusions in corundum from basalts can not only provide information about the physical and chemical conditions of corundum crystallization but also give insight into the processes taken place in the upper mantle. Although current models about the origin of the corundum in alkaline basalt are controversial, there is a consensus that the corundum genesis involves at least two main stages: the first stage when corundum was produced as a magmatic or metamorphic phase at mantle/crustal depth and the second stage when corundum was incorporated into a magma which was transported to the surface via subsequent intraplate alkaline magmatism (Guo *et al.*, 1996; Sutherland *et al.*, 1998; Qiu *et al.*, 2001; Smirnov *et al.*, 2006). In addition, as the corundum has a special capability to withstand high temperatures and pressures due to its high rigidity and melting point, the melt- and fluid inclusions trapped in corudum megacrysts can preserve important information about the conditions of the formation and evolution of the corundum. Therefore, the corundum megacrysts originated from upper mantle and/or lower crust are the ideal samples for the study of deep fluids and melts.

Many studies on the inclusions in basalts have focused on those in olivine, pyroxene and feldspars whereas inclusions in corundum or sapphire received less attention. The Changle area in Shandong has the largest sapphire deposit in China and sapphire/corundum occurs both in Quaternary sediments and in Tertiary basalts. The corundum commonly contains mineral inclusions of Ni-Ta oxides (such as niobite, pyrochlore, ilmenrutile, samarskite, etc.), alkaline-feldspar, low-Ca plagioclase (albite-oligoclase) and zircon with minor Co-rich spinel, Th-Ce-rich phosphate and uraninite. Apart from mineral inclusions, abundant melt inclusions, fluid-melt inclusions and CO_2 fluid inclusions are present in corundum megacrysts in alkaline basalt from this area (Qiu *et al.*, 2001).

Previous studies on the melt inclusions in corundum from the Changle area were focused on the description and identification of daughter minerals in melt inclusions (Guo *et al.*, 1996; Qiu et al, 1999, 2001; Ding, 1998, 1999) and there is no report yet about the high temperature homogenization experiment on them. In this study, observation of phase transitions and high temperature heating experiments of the melt inclusion in corundum were conducted in order to place some constrains on the origin, physical and chemical conditions prevailing during the crystallization of corundum megacryst.

* Corresponding author: E-Mail: peini@nju.edu.cn

1 Geological background

The studied area is located in the northeast segment of the Cenozoic basaltic belt in the east of China, and eruptions of alkaline basalts in the area were controlled by the Yishu fault, the north segment of the Tanlu fault, and the Shangwujing fault of second-order. Argillaceous and sandy limestone and dolomite from the Cambrian to the Ordovician crop out sparsely in the area. The isotopic age data indicate that the eruptions of sodic basaltic magma took place mainly in the early Miocene and Pliocene. Two phases of volcanism which are closely associated with corundum formation produced the Niushan basalt (14.48 ± 0.79Ma) and the Raoshan basalt (4.34 ± 0.19Ma). The former occurs mainly at lap and the bottom (lower horizons) of mountains, consisting of alkaline olivine basalt and basanite, which contain abundant vesicules and mantle xenoliths, with brown mudstone interlayer; the latter is distributed mainly on the top of Fangshan and Beiyan mountains, consisting of horizontal and thick-layered basalt and olivine-pyroxene trachybasalt with minor dolerite (Fig. 1).

Corundum megacrysts in the Niushan alkaline basalt and basanite, are closely associated with mantle xenoliths, consisting mainly of lherzolite with minor harzburgite. The composition of the host basalt is characterized of high contents of (K_2O + Na_2O) (4.46 % ~ 4.92 %), Al_2O_3 (13.05 % ~ 14.15 %) and TiO_2 (1.75 % ~ 3.75 %), low concentration of SiO_2 (43.62 % ~ 47.70 %) (Dong *et al.*, 1999).

Corundum crystals are prismatic and tubbish in shape but some are broken; and the maximum of transection is up to 8cm with an average of 0.5 ~ 2cm. They have no cleavage, but {0001} parting; No = 1.772 ~ 1.775, Ne = 1.764 ~ 1.769; being uniaxial and negative sign in terms of optical properties (Yu 1999).

Most corundum crystals occurred in the studied area are blue-black and dark blue in color; those with medium to light blue color are less common; occasionally yellow corundum can be seen. The light-colored, translucent-to-transparent corundum crystals can be cut for gemstones. They often show hexagonal color patterns with different colors, tones and width of color bands.

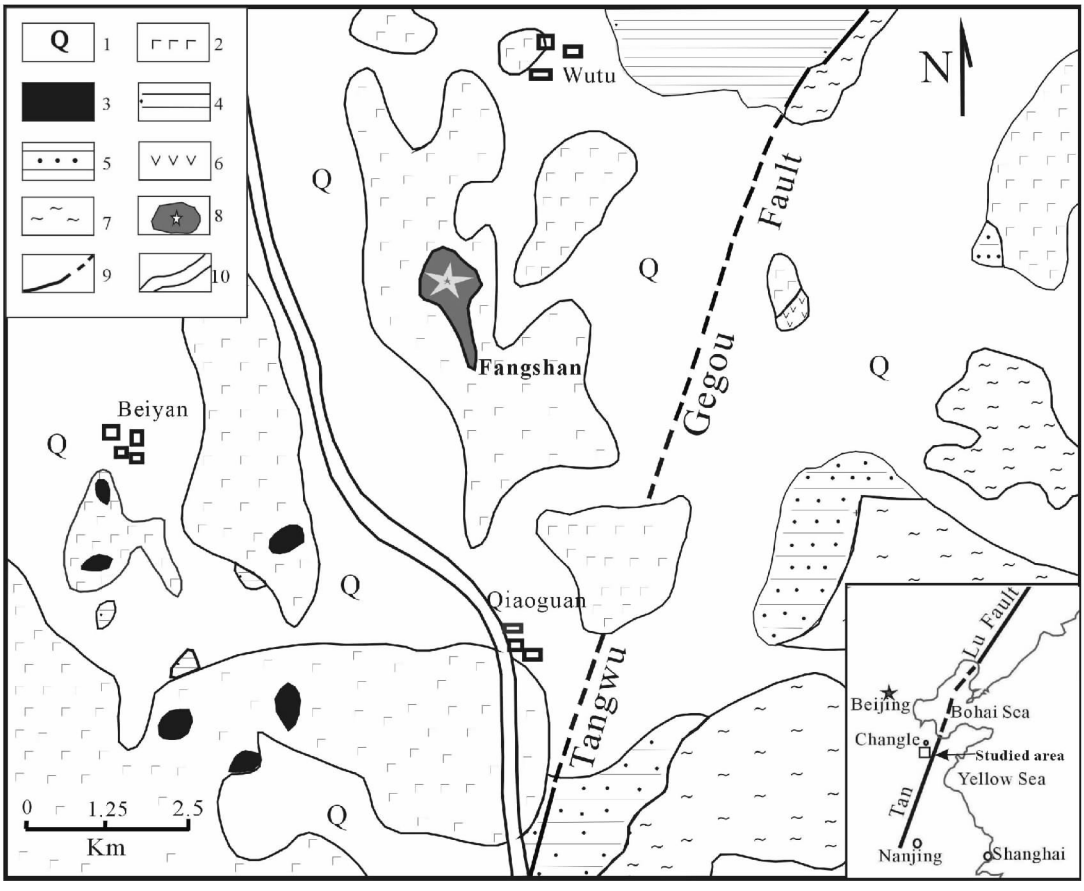

Fig. 1 Geological map of studied area

1-Quaternary alluvium, proluvium and eluvium sediments; 2-late Tertiary Niushan formation (olivine basalt); 3-late Tertiary Raoshan formation (olivine basalt); 4-middle-later Tertiary Wutu formation (shale); 5-Cretaceous Wangshi formation (sandstone with sandy shale); 6-Cretaceous Qingshan formation (intermediate volcanics); 7-Archaean granitic gneiss; 8-corundum producing area; 9-fault; 10-river (modified from Dong *et al.*, 1999 and Zhou *et al.*, 2003)

2 Petrography of melt inclusions

Based on the phases present at room temperature, one type of melt inclusions, i. e. multiphase melt inclusions were identified, which consist of glass phase plus one or more bubbles and daughter minerals. They are ellipsoidal, spherical in shape and vary from 10 to 100μm in size. They occur along the growth zones of host corundum megacrysts. The long-axis of the melt inclusions is perpendicular to or has an angle with the growth zones. The crystalline daughter minerals are short prismatic (Fig. 2A), rod-shaped (Fig. 2B, 2C), acicular (Fig. 2D) with a size of several microns. These daughter minerals are also identified to be Al- and Ca-rich silicate minerals, such as augite and okenite by Laser Raman analysis. The volume percentage of the vapor phase in melt inclusions is different from each other (Fig. 2A, 2B, 2C and 2D).

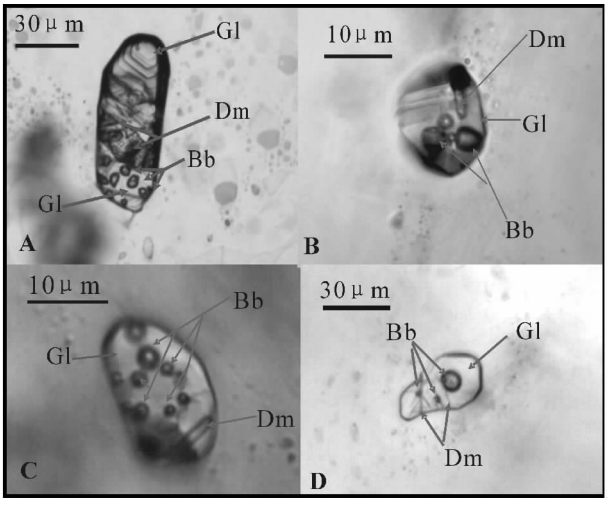

Fig. 2 Characteristics of studied melt inclusions. A-melt inclusion consisting of several deformed bubbles, dark short daughter minerals and residual glass; B-melt inclusion consisting of three bubbles, one short rod-shaped daughter mineral and residual glass; C-melt inclusion consisting of rod-shaped daughter minerals and residual glass, with several (about ten) bubbles; D-melt inclusions consisting of three bubbles, acicular daughter minerals and residual glass. The symbol illumination: Bb-bubble (s); Dm-daughter mineral(s); Gl-residual glass.

3 Analytical Methods

3.1 Sample preparation

Corundum megacrysts were cut and grounded into 0.3mm-thick thin sections which were then polished on both sides. After petrographic observations of melt inclusions the doubly-polished thin sections were immersed in ethanol for 1 ~ 2 days until they can be taken off from carrying glass; the thin sections were, then cleaned, dried and cut into small chips with suitable size for microthermometric measurement of melt inclusions.

3.2 Microthermometric analysis

Microthermometric analysis of melt inclusions was conducted on the LINKAM TS1500 heating stage. The samples prepared as described above were put into sample chamber for homogenization temperature measurement. The phase transition phenomena were observed and recorded using a computer-controlled monitor. Circular water cooling was used during heating experiments. The experiments were accomplished in Fluid Inclusion Lab of the State Key Laboratory for Mineral Deposit Research, Nanjing University.

3.3 Laser Raman microprobe analysis

The bubbles and daughter minerals within the melt inclusions were analyzed by laser Raman microprobe before heating experiments. The analyses were conducted in the State Key Laboratory for Mineral Deposit Research, Nanjing University. All Raman spectra were collected on a Renishaw RM2000 laser Raman microprobe which is fitted with an air-cooled CCD detector. Excitation was achieved using an ionized argon laser (514nm). Wave number measurements were done at 23℃ with the accuracy of $1cm^{-1}$. The laser intensity on the surface of samples is 5mW, slit-width is 50m, grating is 1800, the spectra collecting time is 60s with each measurement being scanned twice.

Table 1 Conditions for microthermometric measurement of the melt inclusion

Heating rate ℃ · min^{-1}	Hold temper ℃	Hold time min	Heating rate ℃ · min^{-1}	Hold temper ℃	Hold time min.
10	100	5	5	750	20
10	200	5	5	800	20
10	300	5	3	850	30
5	400	5	3	900	30
5	450	20	3	950	30
′5	500	20	3	1000	30
5	550	25	2	1050	60
5	600	10	2	1100	40
5	650	10	2	1150	65
5	700	20			

4 Result

4.1 Experiment procedure and phase transitions

The kinetics of melting during the heating experiment is an important issue. If the temperature rises too fast (i. e., the heating rate is higher than the melting rate of solids in the melt inclusion), then the melting process will lag behind, which means that the temperature at which phase transition occurs in the inclusion will be lower than the measured temperature. Thus, rapid heating will result in the phase transition(s) to be observed at a higher temperature than the true one. Slow heating, on other hand, will lead to re-equilibration (i. e., equilibration at conditions different from those at the moment of trapping) of a melt inclusion with its host (Roedder, 1979).

The optimal heating rate in each case depends on the melt composition, the size of the inclusion, the temperature of

experiment, and the type of host mineral. For different host minerals, however, it is necessary to carry out similar kinetic experiments in each case to choose the appropriate rate in the high-temperature range (Sobolev and Danyushevsky, 1994). In our study, the heating rate was controlled as follows (Table. 1): 10℃ min^{-1} from room temperature to 450℃, with extended heating at fixed temperature (at intervals of 100℃) for 5 minutes; 5℃ min^{-1} from 450℃ to 800℃, with extended heating at fixed temperature (at intervals of 50℃) for 10 ~ 30 minutes; 3℃ min^{-1} from 850℃ to 1000℃, with extended heating at fixed temperature (at intervals of 50℃) for 30 minutes; 2℃ min^{-1} from 1000℃ to 1200℃, with extended heating at fixed temperature (at intervals of 50℃) for 30 ~ 60 minutes.

The heating experiments were conducted on the melt inclusions. As shown in Fig. 2, the melt inclusion consists of dark crystalline daughter minerals (Dm), a residual glass (Gl) and several deformed bubbles (Bb). A record of important phase transitions during the entire heating experiment on a representative melt inclusion (Fig. 2A) with negative crystal shape and a size of about 100μm is shown in Fig. 3. During the heating, no change was observed in the inclusion below 400℃ due probably to the high melting point of the silicate glass and daughter minerals. On the further heating, the dark minerals in the inclusion began to melt at about 450℃ and significant melting occurred between 450℃ and 500℃ while volatile components were gradually concentrated to form tens of small globules; the tiny globules (bubbles) were merged to form several large globules at 650℃ ~ 750℃ (Fig. 3B, C and D). Meanwhile the globules were moving towards one end or to the wall of the inclusion and dissolved into the melt (Fig. 3D, E, F and G). When the temperature was held at 750℃ for 20 minutes these globules were incorporated into one large globule and three small globules. At 800℃ with extended heating for 15 minutes, these four globules became smaller and clearer, and the daughter minerals in the centre of the inclusion almost melted completely; and only three small dark spots (minerals) remained and disappeared later at about 830 ~ 850℃ while the largest globule (Fig. 3E) dissolved into the melt, leaving only three small globules near one end of the inclusion (Fig. 3F). The inclusion became more transparent at this moment. At 900℃, two acicular daughter minerals, perpendicular to each other in one tip of the inclusion began melting obviously. Meanwhile, the remaining three small globules became even smaller; and one of them turned to a tiny spot at about 940℃ and then disappeared at 950℃ for 14 minutes prolonged heating. At this time, the lower parts of the acicular daughter minerals disappeared whereas its remaining parts continued to melt. Further heating to 1000℃, the remaining daughter minerals disappeared while the two globules shrank continuously. At 1050 ~ 1100℃, the second small globule disappeared slowly, leaving only one small globule. When the last globule disappeared completely at 1150℃, the inclusion was composed of two immiscible melt phases (homogenization). No phase transition was observed with further prolonged heating. Therefore, it is suggested that two immiscible melts coexist at 1150℃. Then the inclusion was quenched at this temperature.

Because the temperature (before quenching) of the circular cooling water in the vessel of pump used during the experiment become higher than that at beginning, the quenching rate is not high enough to quench ideally the melt inclusion. Consequently,

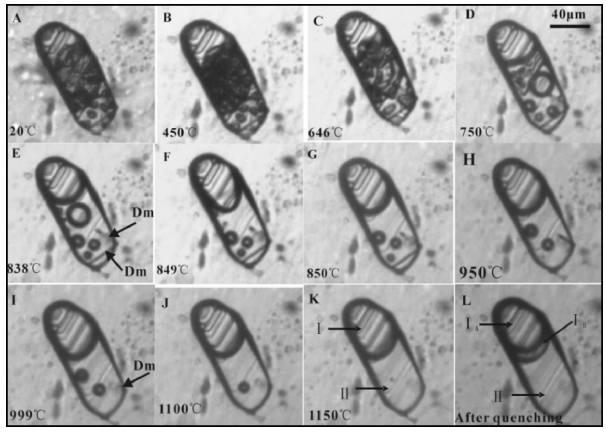

Fig. 3 Photomicrographs showing phase transitions in a melt inclusion in corundum during the heating experiment. A-appearance of an isolated melt inclusion with negative crystal shape at room temperature (20℃); B-small daughter minerals within the melt inclusion started to melt; C-the melted daughter minerals merged into several small globules at about 650℃; D-the small globules were incorporated into four large globules; E-the small globules begun to move and dissolve into melt and remained two acicular daughter minerals; F-the largest globule disappeared into melt at about 849℃; G-after the biggest globule disappeared, the remained globules and the lower daughter mineral gradually became smaller; H-after the lower daughter mineral disappeared, there were only two globules and one daughter mineral at 950℃; I-there were two globules after the last one daughter mineral disappeared at about 999℃; J-the inclusion with only one globule remained at 1100℃; K-after the last globule disappeared, two phases remained at 1150℃; L- because of lower quenching rate, three phases (phase I_A, I_B, Ⅱ) present within the melt inclusion at room temperature after quenching from 1150℃. Illumination: Dm-daughter mineral; the scale bar in the photos is 40μm.

the phase I_A and the phase I_B were separated from the phase I in the melt inclusion after homogenization (Fig. 3L).

4.2 Laser Raman microprobe analysis

The result of laser Raman analysis (Fig4. A, B) of pre-heated melt inclusion was shown in Fig. 4. The pronounced peaks at 1285cm^{-1} and 1388cm^{-1} in the laser Raman spectrum shown in Fig. 4A, indicate that the bubbles in the inclusions contain mainly CO_2, no other component was detected. However clear peaks at 324cm^{-1}, 435cm^{-1}, 664cm^{-1} and 1140cm^{-1} are present in the laser Raman spectrum of daughter minerals in the inclusion (Fig. 4B). On the basis of previous research (Xu and Li, 1996), the peak at 324cm^{-1} coincides with the Raman shift of Al-O band (323cm^{-1}) for beryl and / or Fe^{2+}-O band for jenite. The peak at 435cm^{-1} coincides with the Raman shift of Mg-O band in olivine and peaks at 664cm^{-1} and 1013cm^{-1} coincides with the Raman shift of [SiO_4] chain in pyroxene. Thus, in combination with the Raman shift of OH- band near 3600cm^{-1}, the daughter minerals in the melt inclusion are thought to be hydrous and Fe-Mg silicates, such as augite and/or okenite. Although peaks at 324cm^{-1} and 1140cm^{-1} overlap the

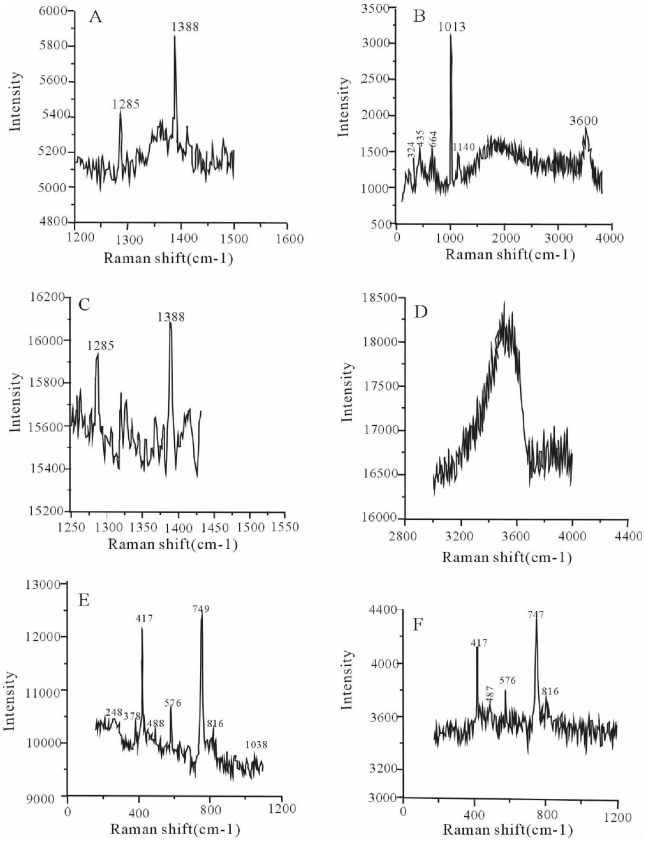

Fig. 4 The laser Raman spectra of melt inclusion. (A) Laser Raman spectrum of the bubbles in melt inclusion (Fig. 2A); (B) laser Raman spectrum of a daughter mineral in melt inclusion (Fig. 2A) prior to reheating; (C) and (D) laser Raman spectra of CO_2 and H_2O dissolved into the volatile-rich melt (phase Ⅰ) in the homogenized melt inclusion after quenching; (E) and (F) laser Raman spectra of phase I_A melt and phase Ⅱ melt in the quenched melt inclusion (Fig. 3. K).

range of Raman shift of PO_4^3 group ($960cm^{-1} \sim 1140cm^{-1}$), no such mineral is recognized, so the peak at $1140cm^{-1}$ is thought to be influenced by [SiO_4] band.

Laser Raman spectra of the quenched melt inclusion are shown in Fig. 4 as well. The Raman spectrum in Fig. 4C confirms that the phase I_A melt is rich in CO_2. This is consistent with the fact that CO_2 fluid inclusions occur in corundum (Qiu *et al.*, 1999), suggesting the presence of CO_2 during the crystallization of corundum. Meanwhile, the pronounced peak of OH band at $3500cm^{-1} \sim 3600cm^{-1}$ in the Raman spectrum of phase I_B (Fig. 4E) confirms that the phase I_B melt is rich in H_2O. On the other hand, the Raman spectrum of the phase Ⅱ melt has only peaks of host corundum without peaks of H_2O and CO_2; this suggests that the phase Ⅱ melt is H_2O- and CO_2-poor (or even absent). Both the Raman spectra with the scanning range of $0 \sim 1200cm^{-1}$ for the phase I melt and that for the phase Ⅱ melt have the peaks of corundum at $417cm^{-1}$, $747cm^{-1}$ (or $749cm^{-1}$) and $816cm^{-1}$; in addition, there are obvious peaks at $488cm^{-1}$ and $576.4cm^{-1}$ (Fig. 4D and 4F), the former lies at the low frequency section of peaks characteristic of the Na_2O-Al_2O_3-SiO_2 system while the latter lies at the peaks characteristic of the Na_2O-SiO_2 system (Xu, *et al.*, 1996). Moreover, the spectrum with scanning range of $0 \sim 1200cm^{-1}$ for the phase I_A melt has characteristic peaks at $378cm^{-1}$ and $1038cm^{-1}$ which do not occur in the spectrum for phase Ⅱ. The former corresponds to the peak of host corundum at about $380cm^{-1}$ while the latter lies at the high frequency section of the peaks characteristic of the Na_2O-Al_2O_3-SiO_2 system (Xu, *et al.*, 1996). The peak at $248cm^{-1}$ may be reflection of the Raman shifts of Mg-O ($299cm^{-1}$) and Ca-O ($224cm^{-1}$). Therefore, the melt trapped in this inclusion in corundum is inferred to be silicate melt of the Na_2O-Al_2O_3-SiO_2 series. The laser Raman spectra of quenched melt inclusion suggest that the phase I melt is rich in CO_2 and H_2O whereas the phase Ⅱ is a silicate melt poor in CO_2 and H_2O.

5 Discussion and conclusion

5.1 Homogenization kinetics

Complication may arise from experimental problems, in particular interaction between silicate melt and host mineral and/or homogenization kinetics. Homogenization kinetics depends largely on the viscosity of silicate melt, the melting rate of daughter mineral and the diffusion rate of volatile (e. g., hydrogen) in the inclusions (Frezzotti, 2001). In general, the faster of the heating rate, the higher of the apparent homogenization temperature is attained due to the effect of melting rates of daughter minerals and diffusion of volatiles. The maximum heating rate during the experiment should be equal to the dissolution rate of daughter minerals. Moreover, the time when inclusion needed to achieve homogenization has a positive correlation with viscosity of silicate melt, the larger the viscosity, the more time is needed to achieve homogenization (Xia, 1984). Thus, the melt inclusions should be kept at the temperature close to the homogenization for ca. 30 minutes to 1 hour during experiments.

Homogenization temperatures of melt inclusion can be influenced obviously by dissociation of water and hydrogen diffusion. Dissociation of H_2O in melt inclusion will raise the homogenization temperature (Sobolev and Danyushevky, 1994). As the effect of H_2O dissociation on larger inclusions is small (Sobolev and Danyushevky, 1994) and melt inclusions larger than 50 m were used in this study, the effect of H_2O dissociation on the homogenization temperature can be neglected.

The heating rate adopted in our study (see Table. 1) is 2℃/min to 5℃/min, which is the desirable heating rate for most melt inclusion microthermometry study in basaltic rocks. The 1℃/s to 1℃/min heating rates was ever suggested by Danyushevsky *et al.* (1992) for the heating run of melt with ultramafic to basaltic compositions. The rate of 2℃/min was used by Sobolev *et al.* (1988) when doing the homogenization experiments on melt inclusion in high-alumina magnesian basalt from the mid-oceanic ridges. The rate of 2℃/min to 5℃/min were also adopted by Danyushevsky *et al.* (2002) when studied melt inclusions in plagioclase phenocrysts from MORB.

The homogenization temperature (1150℃) obtained by this experiment is reliable, which is supported by the formation temperature of basalt in this area deduced from mineral thermometer ($T = 1100$℃) (Dong *et al.*, 1999). Which is also consistent with homogenization temperatures (1100℃ ~ 1250℃) of basaltic melt inclusions summarized by Danyushevsky, *et al.*

(2002) and in accordance with the generation temperatures of basaltic magma obtained by petrological experiments (Winter, 2001).

5.2 Magma immiscibility

Magma immiscibility (unmixing of melt/melt or melt/fluid) refers to the coexistence, at equilibrium, of two or more magmas (melts and/or fluids), differing in properties and generally in composition (Lu *et al.*, 2004). Magma immiscibility should occur almost inevitably at some point in the evolution of most mantle and crustal-derived magmas during cooling and crystallization. The morphological evidence of immiscibility is always the same: a droplet (globule) of one phase within another of contrasting composition. Roedder (1992) summarized various magmatic immiscibility during the evolution of magma recorded by melt inclusions: silicate melt-dense CO_2 fluid, silicate melt-sulfide melt, silicate melt-silicate melt, silicate melt-low density vapor, silicate melt-carbonate melt, and various types of immiscibility involving silicate melt/hydrous saline melt/aqueous fluid/CO_2 fluid. An immiscibility of silicate melt (poor in volatiles)-silicate melt (rich in volatiles) is described in this paper.

When two or more melt (and/or fluid) phases coexist around growing crystals (magmatic immiscibility), a heterogeneous mixture may be trapped with various ratios of the coexisting phases in different inclusions (Frezzotti, 2001). Coexisting of the volatile-poor silicate melt (phase Ⅱ) with the volatile-rich melt (phase Ⅰ) in one melt inclusion is the direct evidence for immiscibility at high temperature (1150℃). This demonstrates that the two melts coexisted in the parental magma at the time when the corundum crystallized, which is similar to that happened in the apatites from ijolite pegmatites from Usaki complex of West Kenya, i.e. coexistence of carbonate-rich and silicate-rich melts, as described by Rankin and Le Bas (1974). This kind of inclusions can provide direct information of chemical nature at magmatic stages (Frezzotti, 2001).

Acknowledgement This work was supported by National Natural Science Foundation of China (Grant No. 402213101). Thanks are given to two reviewers for their constructive comments and suggestions.

References

Danyushevsky LV, Sobolev AV and Konomkova NN. 1992. Methods of studying magma inclusions in minerals during investigations on water-bearing primitive mantle melts (Tonga trench boninites). Geochem. Int., 19: 48 – 62

Danyushevsky LV, McNeill AW, Sobolev AV. 2002. Experimental and petrological studies of melt inclusions in phenocrysts from mantle-derived magmas: an overview of techniques, advantages and complications. Chemical Geology, 183: 5 – 24

Dong ZX, Yang LF, Wang YW. 1999. Study on the origin of the sapphire deposit in the Changle area, Shandong. Acta Geoscientia Sinica, 20(2):177 – 183 (in Chinese with English abstract)

Ding ZH. 1998. Inclusions in corundum megacryst from alkaline basalt I: The discovery of oligoclase inclusions and its significance. Acta Mineralogica Sinica, 18(1): 23 – 26 (in Chinese with English abstract)

Ding ZH. 1999. Study on inclusions in megacryst corundum from Shandong province II: Chloride and the composition of mantle liquid. Journal of Mineralogy and Petrology, 19(1): 15 – 18 (in Chinese with English abstract)

Frezzotti ML. 2001. Silicate-melt inclusions in magmatic rocks: application to petrology. Lithos, 55: 273 – 299

Guo J, O'Reilly SY, Griffin WL. 1996. Corundum from basaltic terrains: a mineral inclusion approach to the enigma. Contrib. Mineral. Petrol., 122: 368 – 386

Lu HZ, Fan HR, Ni P *et al.* 2004. Fluid Inclusions. Beijing: Science Press, 356 – 362 (in Chinses)

Qiu ZL, Chen JD, Chen BH, Zhu M. 2001. The Forming of Corundum megacrysts related to alkali basalt in Changle, Shandong. Acta Scientiarum Naturalium Universitatis Sunyatseni, 40(2): 107 – 111 (in Chinese with English abstract)

Qiu ZL, Chen BH, Chen JD. 1999. Discovery of Zircon inclusions in corundum megacrysts related to alkli basalt in Changle, Shangdong. Acta Scientiarum Naturalium Universitatis Sunyatseni, 38(6): 131 – 132

Rankin AH and Le Bas MJ. 1974. Liquid immiscibility between silicate and carbonate melts in naturally occurring ijolite magma. Nature, 250: 206 – 209

Roedder E. 1992. Fluid inclusion evidence for immiscibility in magmatic differentiation. Geochim. Cosmochim. Acta, 56: 5 – 20

Roedder E. 1979. Origin and significance of magmatic inclusion. Bull. Mineral., 102: 487 – 510

Sutherland FL, Paul WO, Hoskin C, Mark Fanning, Robert R Coenraads. 1998. Models of corundum origin from alkali basaltic terrains: a reappraisal. Contrib. Mineral. Petrol., 133: 356 – 372

Smirnov SZ, Izokh AE, Kovyazin SV, Hoa C *et al.* 2006. Inclusions in the Dak-Nong placer sapphires: Conditions of corundum crystallization in the Middle Vietnam Earth Crust (Abstract)

Ni P and Li ZL (eds.). 2006. ACROFI I, Nanjing, China. Nanjing University, 200 – 202

Sobolev AV, Danyushevsky LV, Dmitriev LV, Suschevskaya NM. 1988. High-alumina magnesian tholeiite as one of primary basalt melts of basalts of the mid-oceanic ridges. Geokhimiya, 10: 1522 – 1528 (Translated into English in Geochem. Int., 1989, 26: 128 – 133)

Sobolev AV, Danyushevsky LV. 1994. Petrology and geochemistry of boninites from the north termination of the Tonga Trench: constraints on the generation conditions of primary high-Ca boninite magmas. J. Petrol., 35: 1183 – 1211

Winter JD. 2001. An Introduction to Igneous and Metamorphic Petrology. New Jersey: Prentice-Hall Inc

Xia LQ. 1984. Kinetic behaviour of homogenization process of silicate melt inclusions. Scientia Geologica Sinica, (3): 323 – 329 (in Chinese)

Xu PC, Li RB *et al.* 1996. Raman Spectroscopy in Geosciences. Xi'an: Shanxi Press of Science and Technology (in Chinese)

Yu XY. 1999. Jewel mineral characteristic of sapphire from Shandong province. Rocks and Mineral Analysis, 18(1): 41 – 45 (in Chinese with English abstract)

Zhou DS, Liu JT, Yang DR, Zhang PQ. 2003. Geological characteristics of sapphire deposit in Changle of Shandong province. Geology of Shandong Province, 19(2): 26 – 29 (in Chinese with English abstract)